Predicting the Activity of Boronate Inhibitors Against Metallo-β-lactamase Enzymes

Elena O. Levina[1], **Maria G. Khrenova**[1,2], **Vladimir G. Tsirelson**[1,3]

Potency of boronate inhibitors against metallo-β-lactamases (MβLs) has been found to be dependent on the electrophilicity of the boron atom. It forms a covalent bond with the oxygen atom of the catalytic OH^- ion in the active site of the enzyme. The ability of the boronate inhibitor to influence the protein conformation also affects the binding potency. Molecular dynamics (MD) simulations of cyclic and non-cyclic boronate complexes with NDM-1 MβL show their higher impact on the inhibitor efficiency compared with the electrophilicity of the boron atom. Therefore, we focus on the hardware impact on the computational speedup of the GPU-accelerated MD. Using this data, we propose a comprehensive protocol for *in silico* prediction of the activity of boronate molecules against MβL enzymes, which includes MD simulations, combined quantum mechanics / molecular mechanics (QM/MM) computations and molecular dynamics simulations with the QM/MM potentials (QM/MM MD).

Keywords: metallo-β-lactamase, boronate inhibitors, MD, QM/MM MD, quantum theory of atoms in molecules (QTAIM), GPU-accelerated algorithms.

Introduction

Nowadays, one of the most severe threats to the healthcare system is a dramatic spread of antibiotic resistant bacteria which have flourished enormously over several decades. Resistance to β-lactam antibiotics via production of β-lactamases by infectious agents is an extremely common type of resistance mechanism [52]. Situation is exacerbated by the structural diversity of β-lactamases, which utilize different mechanisms of β-lactam hydrolysis depending on the structure of their active sites [7, 8]. Serine β-lactamases covalently bind antibiotic via serine residue and perform acylation/deacylation reactions, while metallo-β-lactamases (MβLs) utilize Zn^{2+} cations to coordinate β-lactam molecule in their active site and then cleave the β-lactam four-membered ring by the OH^- nucleophilic attack. It significantly complicates the search for broad-spectrum inhibitors restoring β-lactam activity against resistant pathogens, regardless of the hydrolysis mechanism they use [40].

Recently, United States Food and Drug Administration and European Medicines Agency approved vaborbactam as a first boronate inhibitor of β-lactamases [28, 50]. Despite its ability to inhibit serine β-lactamases, this compound had no activity against MβLs [28]. It provoked extensive research of boronate compounds active against the entire β-lactamase family. The number of potent inhibitors has been proposed [9, 26, 41, 42, 58], including promising QPX7728 compound with remarkably broad spectrum of inhibition [20, 29, 53]. However, since even the first phase of its clinical trials has not yet been completed [2], there is still need in the research of other boronates effective against MβLs [36, 45]. In this regard, it is especially important to find protocols for *in silico* prediction of the boronate activity.

In this study, we have focused on the several non-cyclic and cyclic boronates having different activity against NDM-1 MβL (Tab. 1). NDM-1 is an enzyme provoking a great concern due to its ability to hydrolyze last-resort carbapenem antibiotics and progressing spread over the

[1]A.N. Bach Institute of Biochemistry, Federal Research Centre "Fundamentals of Biotechnology" of the Russian Academy of Sciences, Moscow, Russia
[2]Department of Chemistry, Lomonosov Moscow State University, Moscow, Russia
[3]Mendeleev University of Chemical Technology, Moscow, Russia

world [12, 28, 37, 39, 51]. It has been an ideal object for studying the features of boronate inhibition of metalloenzymes, a complex reversible process [49, 53]. Its mechanism is based on the boronate inhibitor ability to bind the catalytic OH^- ion to its boron atom and possibility of temporally prevention MβL from restoring its activity by occupying the enzyme active site via Zn^{2+} coordination (Fig. 1). Two different factors should be of paramount importance in this process: the reactivity of the boronate fragment and the tendency of the inhibitor to dissociate from the enzyme. We aimed to investigate the particular reasons for the increased activity of the cyclic boronates against NDM-1 in comparison with their non-cyclic analogs and the reasons for different inhibitory activity among the cyclic boronates themselves. Our study showed that this requires taking into account the dynamic properties of the systems under consideration, hence, we were also interested in optimizing time-consuming calculations needed for their evaluation. For this purpose, we used GPU-accelerated computations and focused on the hardware impact on their speedup. Thus, our goal was to offer a comprehensive methodology for the prediction of a boronate inhibitor activity against a metallo-β-lactamases, both in terms of the computational protocol and hardware choice.

Table 1. Structures of proposed boronate inhibitors of NDM-1 with different activity against the enzyme. Vaborbactam was included as an example of a compound structurally similar to cyclic boronates that lacks activity against NDM-1. Inhibitor activity is expressed as: (i) K_i value determined with imipenem as a substrate [20]; (ii) IC_{50} value measured with cephalothin for the non-cyclic inhibitor [46] or imipenem for the QPX7728 [53]; (iii) a minimum concentration of the inhibitor (C_{inh}) needed to reduce the MIC of the biapenem to the concentration that corresponds to the PK-PD breakpoint for that β-lactam based on human dosing (potential target value or PTV) [20]

Type	Name	Structure	IC_{50}, μM	K_i, μM	C_{inh}, μg/L
Non-cyclic	–		60.7 ± 11.8	–	–
Cyclic	QPX7728		0.055 ± 0.025	0.032 ± 0.014	0.6
	1		–	–	0.6
	2		–	–	20
	Vabor-bactam		–	> 40	–
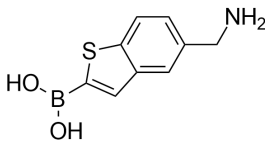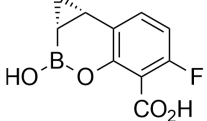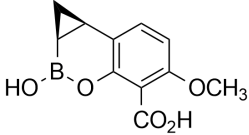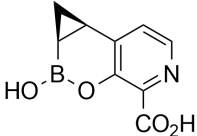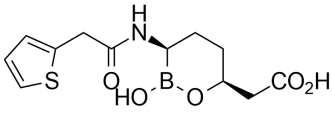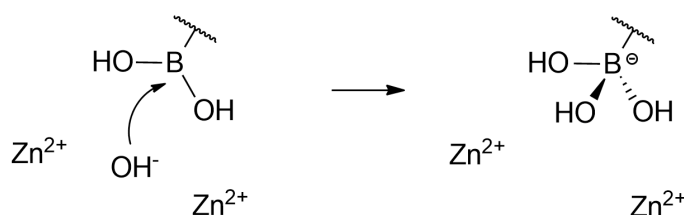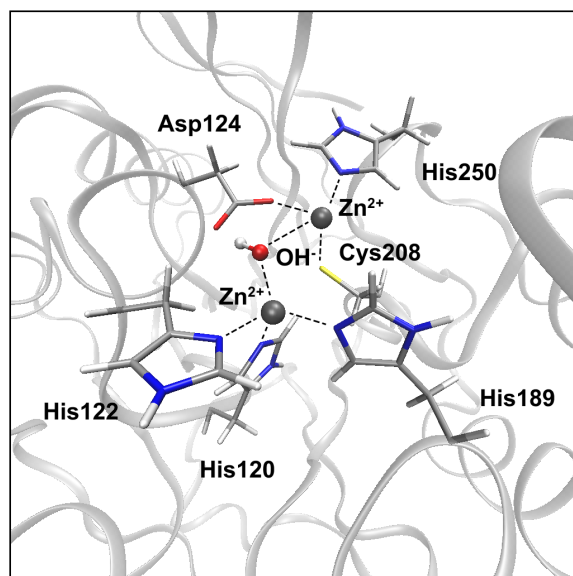
Figure 1. Metallo-β-lactamase (NDM-1) active site and the mechanism of metallo-β-lactamase inhibition by the boronate inhibitors. On the upper frame carbons are shown in silver, nitrogens are in blue, oxygens are in red, sulfurs are in yellow and Zn^{2+} ions are depicted as big grey spheres

1. Methodology

To understand origins of different activity of the boronate inhibitors against NDM-1, chosen cyclic and non-cyclic compounds (Tab. 1) were studied at various theoretical levels. We examined features of their binding with the enzyme using molecular dynamics (MD) and combined quantum mechanics / molecular mechanics (QM/MM) simulations. The dynamic changes in chemical properties of the boronate molecules were studied using a molecular dynamics simulation with the QM/MM potentials (QM/MM MD) of boronates in water solution.

The MD computations were performed for the complexes of the QPX7728 and non-cyclic boronate with NDM-1. Their crystal structures (PDB IDs: 6V1M [20] and 6Q2Y [10]) were taken as a starting point for the construction of the model systems. Both systems were solvated in the rectangular water box (distance from the protein to the cell border equaled 15 Å) and neutralized. After energy minimization and preliminary 20 ns MD simulation with fixed atomic positions of the inhibitor attacked by the OH^-, Zn^{2+} ions and protein L3 loop (Leu65–Val73), the 500 ns simulation was carried out in the NAMD program package [43, 44]. The NPT ensemble

was chosen with T = 300 K, p = 1 atm and 1 fs integration step. The information about system energy, coordinates and velocities has been written every 0.05 ns. The CHARMM36 force field parameters [6, 23, 31, 32] were chosen for the ions and protein atoms, while the TIP3P parameters [25] were used for the water molecules. The inhibitors with bonded OH^- were described by the CGenFF parameters [55, 60], while their atomic charges were reparametrized via electrostatic-potential-charge derivation procedure using RED Server interface [3, 13, 56] (based on the Gaussian 09 [1] calculations). This methodology has already proven to be effective for the reparameterization of other boronate molecules [57]. The obtained trajectories were analyzed via VMD program [24] and MD Analysis Python library [16, 35].

The QM/MM simulations were performed for the complexes of cyclic inhibitors with the bacterial enzyme. First, the local minimum on the potential energy surface (PES) was located for the QPX7728 complex with NDM-1, then it was modified and reoptimized for other inhibitors. In all cases, the attainment of the PES minimum was confirmed by the analysis of the IR harmonic frequencies. The QM/MM calculations for the QPX7728-protein complex started from the structure, obtained in the preliminary 20 ns MD simulation, with reduced water shell of the model system (8710 atoms in total). The QM part of each model consisted of the inhibitor molecule attacked by the OH^-, Zn^{2+} ions and amino acid residues bonded either with zinc cations, or with inhibitor (His120, His122, Asp124, His189, Cys208, Gly219, Asn220, His250) and several water molecules interacting with the inhibitor. These subsystems were described at the PBE0-D3/6-31G(d,p) level of theory [4, 18, 19, 21], while the MM subsystems were modeled with the AMBER force field parameters [11]. The electronic embedding scheme was applied assuming contributions of the partial charges from all MM atoms to one-electron part of QM Hamiltonian. For the QM/MM simulation itself, the NWChem program package [54] was utilized, while the subsequent quantum-topological analysis of electron density for the QM subsystems was performed in the Multiwfn program [30].

The QM/MM MD simulations of the water solutions of boronate molecules were carried out via interface [34] for the NAMD [43, 44] and TeraChem [47] software, which perform the classical MD and quantum chemical calculations, correspondingly. The inhibitor structures were obtained from the QM/MM calculations (for the non-cyclic inhibitor we used results obtained in our previous work [27]), then each system was solvated in the rectangular water box (distance from the inhibitor to the cell border equaled 15 Å) and neutralized. The preliminary 2 ns MD computation was performed before the 15 ps QM/MM MD simulation. The QM part included only the inhibitor molecule and was described at the PBE0-D3/6-31G(d,p) level of theory, while MM part contained water molecules with TIP3P parameters. Similarly, to the MD simulations, the NPT ensemble was chosen. The information about system energy, coordinates and velocities has been written every 1 fs. At the step of data analysis, first 5 ps of simulations were excluded from consideration. The atomic Fukui electrophilicity indices [38] were calculated using Hirshfeld charges [22] for 100 frames from QM/MM MD trajectory using Multiwfn code [30].

The benchmark studies were carried out for the MD simulations, since they were the most time-consuming part of all computations. The computational protocol was identical to the one used for the examination of NDM-1 conformation in its complex with the cyclic QPX7728 inhibitor. All other information, including the hardware specifications and the benchmark results, is discussed in the Section 2.3.

2. Results and Discussion

2.1. Cyclic and Non-cyclic Boronate Activity

The direct comparison of the NDM-1 crystal structures with cyclic (compound QPX7728) and non-cyclic boronate inhibitors (Tab. 1) demonstrate different location of the inhibitor molecule in the enzymatic active site (Fig. 2). The QPX7728 is located more closely to the L3 (Leu65–Val73) and L10 (Asp225–Asp254) loops, while its non-cyclic analog is directed outward the active site cavity. One can speculate that these distinctions in the orientation of the inhibitors can affect the dynamical behavior of the protein loops and, as a consequence, influence the stability of the enzyme-inhibitor complex.
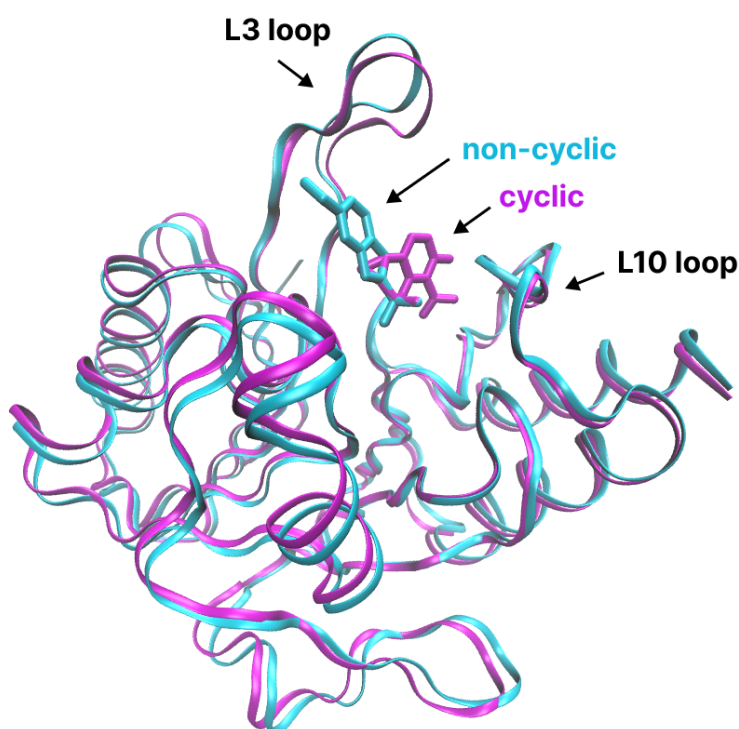
Figure 2. Alignment of the crystal structures of the NDM-1 with the cyclic QPX7728 and non-cyclic boronate (PDB IDs: 6V1M [20] and 6Q2Y [10], correspondingly). $IC_{50} \approx 55$ nM for the QPX7728 [53] and 61 μM for the non-cyclic inhibitor [46]

The results of the molecular dynamic simulation showed that both enzymes do not change conformation dramatically along the trajectory (Fig. 3 first panel). However, the RMSD for the complex with the non-cyclic inhibitor is substantially flatter than for the complex with the cyclic boronate. For the non-cyclic inhibitor, RMSD of the protein backbone vary within 1 Å, while for the cyclic one the minimum and maximum values are separated by 2 Å. This suggests that non-cyclic boronate induces higher stabilization of the flexible protein loops. To find out what structural movements are causing the RMSD bumps for the complex with the cyclic boronate, we performed a principal component analysis (PCA). It turned out that no principal component contains a large part of the overall fluctuations of the protein backbone (Tab. 2): first six components account for 50% of the total variance, while twenty PCs are needed to achieve 75%. These results confirm that overall protein has a stable conformation along the trajectory and RMSD variation is caused only by the movements in its flexible parts. Since each of the first

Table 2. The percentage of total variance, which is accounted for individual PCs and their cumulative variance

PC number	PC variance, %	Cumulated variance, %
1	16.0	16.0
2	12.2	28.2
3	8.6	36.8
4	6.5	43.3
5	4.7	48.0
6	3.4	51.4
7	3.0	54.4
8	2.3	56.7
9	2.3	59.0
10	2.0	61.0
11	1.7	62.7
12	1.6	64.3
13	1.6	65.9
14	1.3	67.2
15	1.1	68.3
16	1.2	69.5
17	1.0	70.5
18	0.9	71.4
19	0.9	72.3
20	0.9	73.2

two components contains more than 10% of the overall fluctuations, they were inspected more closely than others.

The PC1 motion is mainly connected with the L3 loop conformational changes and some motions at the bottom of the enzyme (far from the active site). At the 50 ns the L3 loop is maximally open, which corresponds to the minima in the amplitude of the fluctuations along the PC1 (Fig. 3, second panel). The pronounced RMSD peaks between 280 and 430 ns are also in the good agreement with the fluctuations along the PC1 and correspond to the loop "widening" (Fig. 3, second panel). The PC2 captures this "widening" as well, but does not reflect loops opening-closing motions. Fluctuations along the PC2 are mainly associated with N-terminus motion and are clearly visible in the 50–280 and 440–500 ns regions on the RMSD graph. Among other components that yield 5–8% of total variance (Fig. 4), only the fluctuations along the PC3 are partly connected with protein movements in the vicinity of the active site. Similar to the PC1, PC3 captures loop opening at $\sim$ 50 ns and its closing at $\sim$ 100 ns and some opening-closing movements around 400 ns. The visual inspection of the enzyme complex with non-cyclic inhibitor confirms that, in contrast to the complex with cyclic QPX7728, protein loops are less tended to change conformation. Notably that the L3 loop is almost always open along the simulation. Thus, the conducted analysis reveals that part of the RMSD variance along the trajectory for NDM-1 complex with cyclic boronate is rooted in the L3 loop movements, which is more flexible than for the structure with the non-cyclic boronate inhibitor.
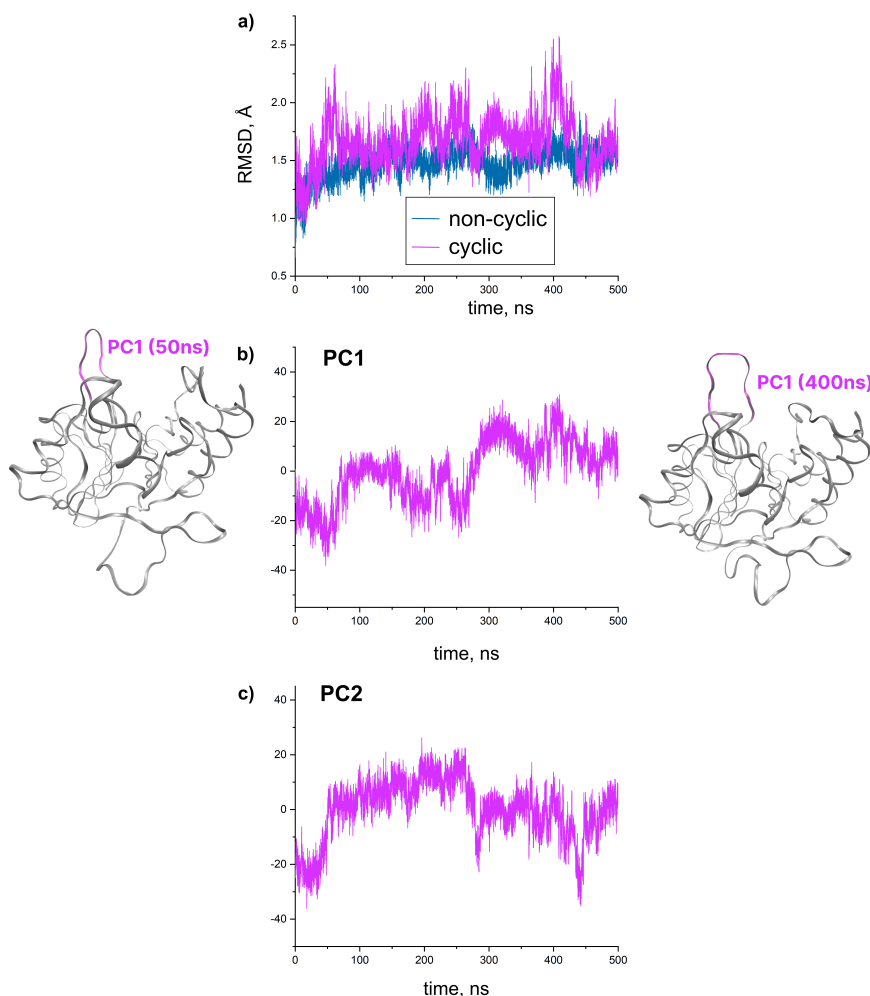
Figure 3. The two first principal components calculated for the trajectory of NDM-1 with the cyclic QPX7728 inhibitor and RMSD for the enzymatic complexes of cyclic and non-cyclic boronates

The L3 loop, which movement is affected by the type of a boronate in the NDM-1 active site, consists of the Leu-Asp-Met-Pro-Gly-Phe-Gly-Ala-Val sequence. Thus, one can suppose that the bulky Phe70 interacts with the inhibitor when the loop is closed and serves as an obstacle to the inhibitor trying to leave the active site. To test this hypothesis, we compared the distance between the Phe70 side chain and the cyclic and non-cyclic boronates in the complexes with NDM-1. Since inhibitors have different positions in the NDM-1 active site (Fig. 2), we considered the distance between the Phe70 and both center-of-mass of the inhibitors and position of the boron atom itself, which is roughly the same for these two compounds. The obtained graphs (Fig. 5) clearly indicate that the Phe70 residue is located far from the non-cyclic boronate during simulation, except brief moments in the beginning of the trajectory and around 345 ns.

The inhibitor – Phe70 distance fluctuating around 25 Å for the complex of the non-cyclic boronate with NDM-1 testifies that the L3 loop is fixed in an open conformation. Hence, it cannot prevent the inhibitor from leaving active site. In the case of the cyclic boronate complex with NDM-1, the opening of the L3 is comparable to its opening in the case of the non-cyclic inhibitor only once per trajectory – at times close to 50 ns. All the rest of the time, it either
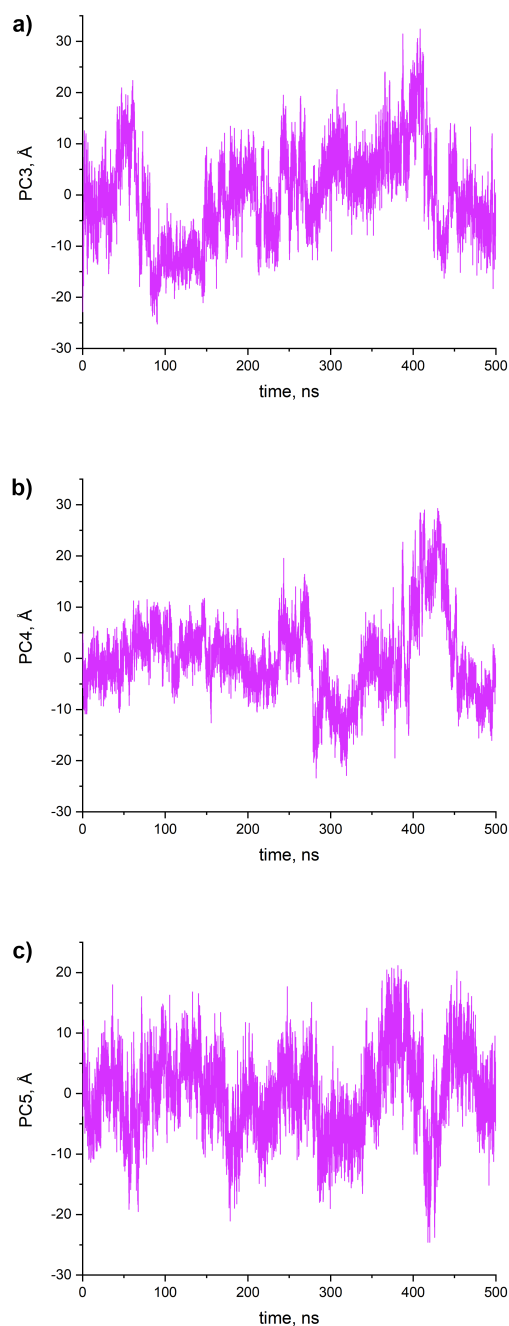
Figure 4. The principal components, which yield ~ 5–8% of total variance (see Tab. 2), calculated for the trajectory of NDM-1 with cyclic QPX7728 inhibitor

oscillates around 15 Å from the inhibitor (opening and closing), or it is stably closed above the active center (at the beginning of the trajectory or in the interval of 80–150 ns).

Such L3 loop behavior can definitely affect a potency of the boronate inhibitor against NDM-1. However, the inhibitor activity can be also dependent on the ability of the boronate fragment to bind catalytic OH^- ion in the enzyme active site (the boron atom electrophilicity) [27]. This raises a question whether the boron atom electrophilicity contribute to the enhanced activity of cyclic inhibitor against NDM-1 or its ability to adjust protein conformation is more important?
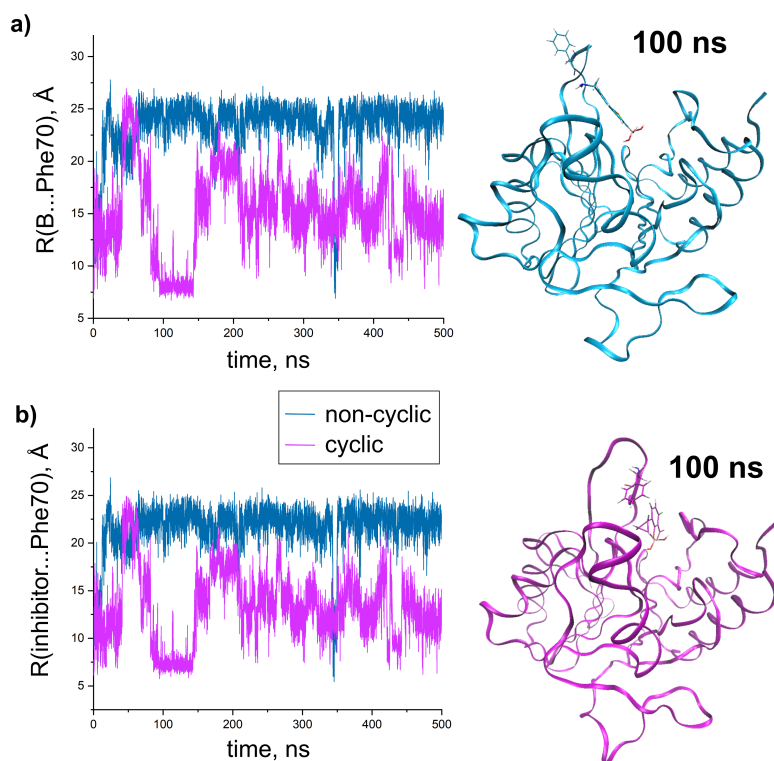
Figure 5. The distance between the center-of-mass of the phenyl ring in the Phe70 residue and a) the boron atom in the non-cyclic and cyclic (QPX7728) inhibitors, or b) the center of mass of the entire inhibitor. The snapshots on the right demonstrate conformations of the L3 loop and Phe70 for NDM-1 complexes with non-cyclic and cyclic inhibitors

From the computational point of view, the electrophilicity can be easily estimated via conceptual DFT approach, which defines the atomic Fukui electrophilicity indices, $f+$, as a difference of the Hirshfeld atomic charges in the N and N+1 electronic states. However, this property of a boron atom is not a "static" one, and in order to argue about its greater or lesser value, it is necessary to consider numerous conformations of the inhibitors in water solution. The obtained distributions (Fig. 6) clearly demonstrate that non-cyclic boronate has more electrophilic boron atom despite its small potency as an MβL inhibitor. Therefore, we can conclude that differences in the IC_{50} values by three orders for non-cyclic and cyclic inhibitors (Tab. 1) are caused by the dynamics of the L3 loop in the NDM-1 complex. The improved inhibitory activity of the cyclic boronate is explained by the tendency of this loop to cover NDM-1 active site, while for the non-cyclic boronate the active site stays open.

2.2. Origins of the Different Activity of the Cyclic Boronates

In contrast to the results of the previous section, differences in the inhibitory activity among the cyclic inhibitors (Tab. 1) cannot be explained by their influence on the enzyme conformation. It can be easily demonstrated by the superimposition of their structures, obtained in the QM/MM simulations (Fig. 7). All complexes of the QPX7728 derivatives with NDM-1 overlap perfectly with each other and no changes in the protein flexible regions are visible.

Despite the fact that cyclic inhibitors are similarly located in the active site, they differently interact with Zn^{2+} ions and amino acid residues of NDM-1 (Tab. 3). It can be revealed by the
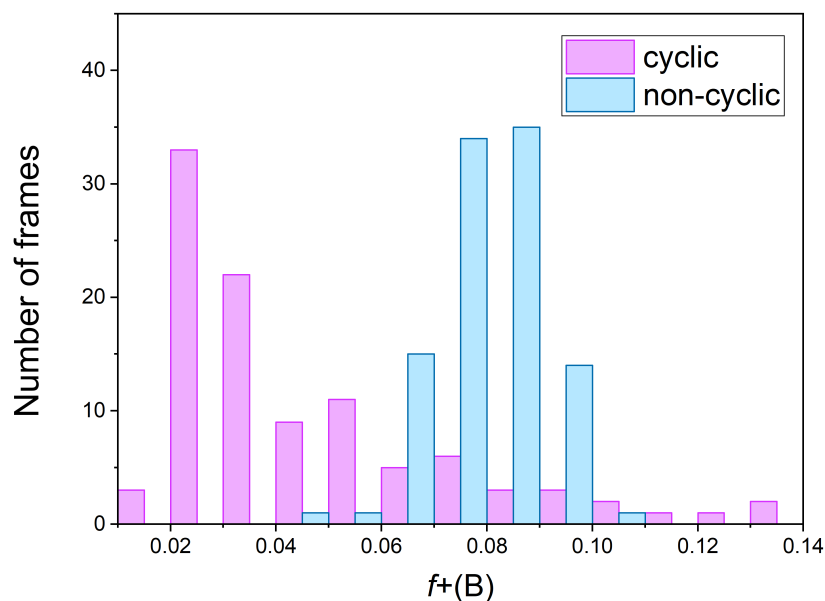
Figure 6. Distributions of the Fukui electrophilicity indices of the boron atom, $f+(B)$, for the cyclic QPX7728 boronate and its non-cyclic analog (Tab. 1) in water solution along the QM/MM MD trajectories. The IC_{50} values are 55 ± 25 nM [53]) for the cyclic inhibitor and 60.7 ± 11.8 μM [46] for the non-cyclic one
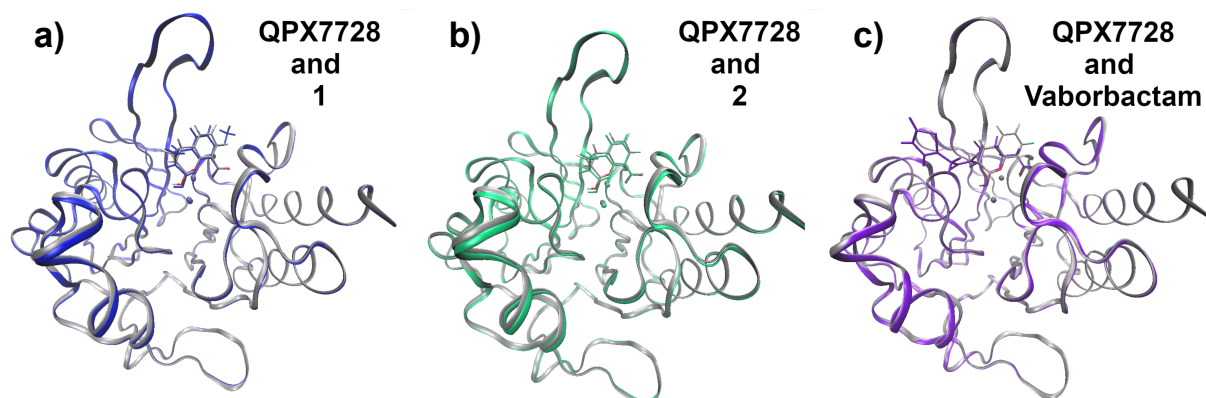
Figure 7. Superimposition of the QM/MM structures of NDM-1 complexes with cyclic boronates (Tab. 1)

quantum-topological analysis of electron density [5], which uses the electron-density saddle points (so-called bond critical points or BCPs) as a marker of the chemical bonding between atoms. This approach also allows one to characterize strength of interatomic interactions [14, 15, 17, 33, 48]. Applying the electron density value at BCP as a simple indicator of the interaction strength, it is easy to see, that despite dissimilarities in the bonding patterns between each of the cyclic inhibitors and protein, all considered compounds have approximately the same binding energy in the active site of the enzyme (Tab. 3). This fact indicates that only the properties of the inhibitor molecule itself can be the source of the different activity of cyclic boronates against NDM-1.

Table 3. Characteristics of intermolecular interactions between cyclic boronate inhibitors and the NDM-1 active site. Distances between inhibitors atoms and Zn^{2+} ions are given in parenthesis if no interatomic interaction was located from topological analysis of electron density. $\Sigma\rho$ stands for the total electron density of the inhibitor-enzyme interactions, which included: (i) contacts between Zn^{2+} ions and a boronate molecule, (ii) conventional hydrogen bonds (H-bonds) between an inhibitor and NDM-1 amino acid residues, and (iii) weak C-H$\cdots$O bonds, between an inhibitor molecule and NDM-1 active site. A schematic representation of a fragment of the boronate molecule involved in the interaction with Zn^{2+} ions is shown in the first row

	QPX7728	1	2	Vaborbactam
R($Zn1^{2+}$…O_1), Å	− (2.7)	2.5	2.6	− (2.9)
R($Zn1^{2+}$…O_w), Å	1.9	1.9	1.9	1.9
R($Zn2^{2+}$…O_1), Å	− (4.1)	− (4.0)	− (4.0)	− (4.0)
R($Zn2^{2+}$…O_w), Å	− (2.8)	2.6	− (2.8)	− (2.8)
R($Zn2^{2+}$…O_2), Å	2.0	2.0	2.0	2.0
R($Zn2^{2+}$…O_3), Å	2.2	2.3	2.2	2.2
$\Sigma\rho$(Zn…inhibitor), a.u.	0.22	0.26	0.25	0.24
$\Sigma\rho$(H-bonds), a.u.	0.16	0.18	0.17	0.16
$\Sigma\rho$(all contacts), a.u.	0.42	0.46	0.45	0.42
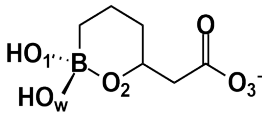
The obtained distributions of the $f+$(B) indices demonstrate that more efficient inhibitors have higher proportion of the conformations with more electrophilic boron atom, then less effective inhibitors (Fig. 8). The most dramatic difference can be seen for the QPX7728 and vaborbactam (Fig. 8b). The extremely low electrophilicity of the boron atom in the vaborbactam explains its zero activity against metallo-β-lactamases and the presence of inhibitory potential against serine β-lactamases. Indeed, in contrast to serine β-lactamases, in metallo-β-lactamases the boronate inhibitor does not covalently bind to the enzyme. After its reaction with OH^- inhibitor can leave the enzymatic active site, while the metallo-β-lactamase can restore its activity. To prevent this, the metallo-β-lactamase inhibitor must have a high electrophilicity of the boron atom in order to immediately bind its other molecule in the active site of the enzyme.

2.3. MD Benchmark Studies

The MD simulations of the complexes of boronate inhibitors with NDM-1 were found to be the most expensive part of our study of inhibitors activity. It was caused not by the cost of the computations themselves, but by the size of the systems under consideration and the trajectory lengths. Therefore, to optimize this part of the protocol for *in silico* prediction of inhibitors activity against metallo-β-lactamases, we performed a benchmark study to select
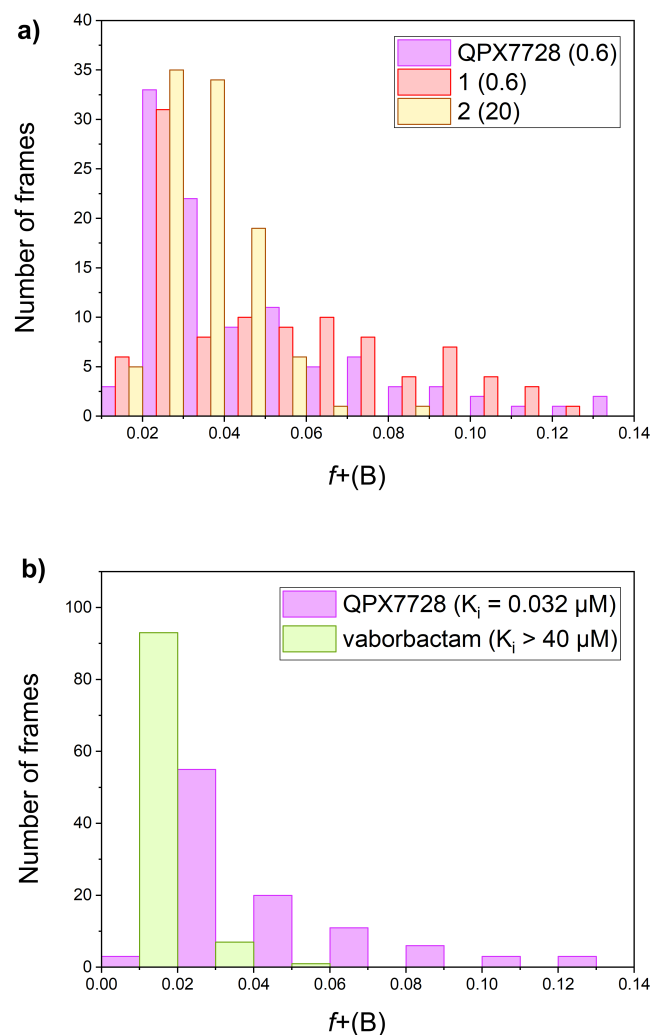
Figure 8. Distributions of the Fukui electrophilicity indices of the boron atom, $f+(B)$, for the cyclic boronates in water solution along the QM/MM MD trajectories. Data on inhibitory activity of boronate molecules against NDM-1 [20] are given in parenthesis. On the upper (a) frame it is expressed as the minimum concentration of the inhibitor (μg/mL) needed to reduce the MIC of biapenem to the concentration that corresponds to the PK-PD breakpoint for that β-lactam based on human dosing

the optimal but widely available hardware for the MD simulation speedup. We examined the QPX7728 complex with NDM-1 in water solution, a system which contained 42938 atoms in total (see Section 1 for the computational protocol) and tested 4 GPUs (Tab. 4 and Tab. 5) with AMD Ryzen Threadripper 1950X and AMD Ryzen 9 3900X CPUs. The NAMD program package was chosen since it is a popular code for MD simulations of large biomolecular systems, which was among one of the first CUDA-accelerated applications. Main hardware and software specifications are presented in Tab. 4 and Tab. 5. Considering benchmark results for NAMD v2 (Tab. 5) one can notice that NVIDIA P102-100 GPU shows the worst results regardless of chosen CPU. The GeForce RTX 3070 and RTX 3070 Ti models demonstrate slight calculation speedup in comparison with GeForce GTX 1070 Ti GPU. However, the crucial improvement in computational speed can be achieved by the optimal hardware/software combination.

Table 4. Main characteristics of the considered NVIDIA GPUs

GPU model	Architecture	Release	Number of cores	Memory, GB	Theoretical performance, GFlops/s		Bandwidth, Gb/s
					SP	DP	
GeForce GTX 1070 Ti	Pascal	2017	2432	8	8186	255.8	256
P102-100	Pascal	2018	3200	5	10770	336.6	440
GeForce RTX 3070	Ampere	2020	5888	8	20310	317.4	448
GeForce RTX 3070 Ti	Ampere	2021	6144	8	21750	339.8	608

Table 5. Benchmark results for the MD simulations of the QPX7728 complex with NDM-1 obtained via NAMD v2 and 3 program [43, 44] with 1 CPU. The main hardware/software specifications are also presented

GPU	CPU	CUDA version	Motherboard	ns / day	
				NAMD v2	NAMD v3
NVIDIA GeForce GTX 1070 Ti	AMD Ryzen Threadripper 1950X	10.0	ASUS PRIME X399-A	10.5	-
NVIDIA P102-100	AMD Ryzen Threadripper 1950X	10.0	ASUS PRIME X399-A	6.4	-
	AMD Ryzen 9 3900X	9.1	ASRock X570 Pro4	7.7	57.8
NVIDIA GeForce RTX 3070	AMD Ryzen 9 3900X	9.1	ASRock X570 Pro4	14.9	81.1
NVIDIA GeForce RTX 3070 Ti	AMD Ryzen 9 3900X	9.1	ASRock X570 Pro4	15.1	84.1

Choosing between 2nd and 2rd version of the NAMD program one should note, that NAMD v2 uses GPU offloading for the force calculations and perform numerical integration on the CPUs. Despite the fact that GPU calculations constitute $\sim 99\%$ of the overall performance, numerical integration can significantly slow down a simulation. The GPU-resident algorithm of NAMD v3 overcome this limitation and results in approximately 5x faster comput-

ing for the Ampere GPUs (Tab. 5). Even a full 12-core CPU load (AMD Ryzen 9 3900X) in the NAMD v2 calculations results only 54.7 ns/day performance (with NVIDIA GeForce RTX 3070 GPU), which is still lesser than for NAMD v3 calculations on GPUs with Ampere architecture. Therefore, the NAMD v3 simulations on modern Ampere GPUs are recommended to achieve maximal acceleration in classical MD simulations.

Conclusion

In this work, we propose a methodology for *in silico* prediction of the activity of boronate inhibitors against metallo-β-lactamase (MβL) enzymes. These compounds reversibly bind Zn^{2+} ions in the MβL active site, capturing catalytic OH^- ion from the MβL. Our study of the NDM-1 inhibition by cyclic and non-cyclic boronates showed that, both enzyme conformation and inhibitors chemical properties can influence molecules potential as an MβL inhibitor. Therefore, combination of various computer simulation methods (classical molecular dynamics, quantum mechanics/molecular mechanics and quantum-classical molecular dynamics) is required to study a potency of these compounds. To speed up some of these computations, we recommend GPU-accelerated calculations and propose detailed protocols for the hardware choice.

Since boronate inhibitors reversibly bind to the MβL, the first step of their activity estimation should include an assessment of their ability to change the conformation of the protein flexible parts near its active site. Classical molecular dynamics (MD) simulations followed by principal component analysis showed that the non-cyclic boronate inhibitor fixes a flexible L3 loop in its open conformation, stipulating its exit from the enzyme. To speed up these expensive calculations one can chose NAMD v3 program package with Ampere GPUs, which demonstrated significant efficiency in this task.

For comprehensive analysis of inhibitor-protein binding, it is desirable to evaluate strength of MβL-inhibitor interactions. It can be achieved by the quantum mechanics/molecular mechanics (QM/MM) calculations followed by the quantum-topological analysis of electron density in the QM part. However, in some cases this step can be omitted, since the protein conformation and properties of the inhibitor molecule were found to have more influence on the inhibitors activity against MβL.

The electrophilicity of the boron atom, which binds catalytic OH^- ion in the enzyme active site, was found to be another aspect capable of strongly influencing the inhibitory activity against MβL. To evaluate this property, one need to perform the quantum-classical molecular dynamics (QM/MM MD) modeling of aqueous solution of the inhibitor, followed by the calculation of the atomic Fukui electrophilicity index, $f+$, for its boron atom along the obtained trajectory. These $f+$ distributions allowed us to interpret different activities of the cyclic boronates against NDM-1, clearly demonstrating that more potent inhibitors are better able to bind OH^- ion in the NDM-1 active site.

Acknowledgements

References

1. Gaussian09, Gaussian, Inc., Wallingford CT, 2016, `https://gaussian.com`

2. P1 Single and Multiple Ascending Dose (SAD/MAD) Study of IV QPX7728 Alone and Combined With QPX2014 in NHV, `https://clinicaltrials.gov/ct2/show/NCT04380207`

3. R.E.D. Server, `https://upjv.q4md-forcefieldtools.org/REDServer-Development/`

4. Adamo, C., Barone, V.: Toward reliable density functional methods without adjustable parameters: The PBE0 model. The Journal of Chemical Physics 110(13), 6158–6170 (1999). `https://doi.org/10.1063/1.478522`

5. Bader, R.F.W.: Atoms in Molecules. Quantum Theory. International series of monographs on chemistry, Clarendon Press (1990)

6. Best, R.B., Zhu, X., Shim, J., *et al.*: Optimization of the additive CHARMM all-atom protein force field targeting improved sampling of the backbone ϕ, ψ and side-chain χ_1 and χ_2 dihedral angle. Journal of Chemical Theory and Computation 8(9), 3257–3273 (2012). `https://doi.org/10.1021/ct300400x`

7. Bonomo, R.A.: β-Lactamases: a focus on current challenges. Cold Spring Harbor Perspectives in Medicine 7(1), a025239 (2017). `https://doi.org/10.1101/cshperspect.a025239`

8. Bush, K.: Past and present perspectives on β-lactamases. Antimicrobial Agents and Chemotherapy 62(10), e01076–18 (2018). `https://doi.org/10.1128/AAC.01076-18`

9. Cahill, S., Cain, R., Wang, D.Y., *et al.*: Cyclic boronates inhibit all classes of β-lactamases. Antimicrobial Agents and Chemotherapy 61(4), e02260–16 (2017). `https://doi.org/10.1128/AAC.02260-16`

10. Cendron, L., Quotadamo, A., Maso, L., *et al.*: X-ray Crystallography Deciphers the Activity of Broad-Spectrum Boronic Acid β-Lactamase Inhibitors. ACS Medicinal Chemistry Letters 10(4), 650–655 (2019). `https://doi.org/10.1021/acsmedchemlett.8b00607`

11. Cornell, W.D., Cieplak, P., Bayly, C.I., *et al.*: A second generation force field for the simulation of proteins, nucleic acids, and organic molecules J. Am. Chem. Soc. 1995, 117, 5179–5197. Journal of the American Chemical Society 118(9), 2309–2309 (1996). `https://doi.org/10.1021/ja955032e`

12. Dortet, L., Poirel, L., Nordmann, P.: Worldwide Dissemination of the NDM-Type Carbapenemases in Gram-Negative Bacteria. BioMed Research International 2014, 1–12 (2014). `https://doi.org/10.1155/2014/249856`

13. Dupradeau, F.Y., Pigache, A., Zaffran, T., *et al.*: The R.E.D. tools: advances in RESP and ESP charge derivation and force field library building. Physical Chemistry Chemical Physics 12(28), 7821–7839 (2010). `https://doi.org/10.1039/C0CP00111B`

14. Espinosa, E., Molins, E.: Retrieving interaction potentials from the topology of the electron density distribution: The case of hydrogen bonds. The Journal of Chemical Physics 113(14), 5686–5694 (2000). https://doi.org/10.1063/1.1290612

15. Espinosa, E., Molins, E., Lecomte, C.: Hydrogen bond strengths revealed by topological analyses of experimentally observed electron densities. Chemical Physics Letters 285(3-4), 170–173 (1998). https://doi.org/10.1016/S0009-2614(98)00036-0

16. Gowers, R.J., Linke, M., Barnoud, J., *et al.*: MDAnalysis: A Python Package for the Rapid Analysis of Molecular Dynamics Simulations. Proceedings of the 15th Python in science conference pp. 98–105 (2016). https://doi.org/10.25080/Majora-629e541a-00e

17. Grabowski, S.J.: Intramolecular Hydrogen Bond Energy and Its Decomposition-O-H· · ·O Interactions. Crystals 11(1), 22935–22952 (2020). https://doi.org/10.3390/cryst11010005

18. Grimme, S., Antony, J., Ehrlich, S., Krieg, H.: A consistent and accurate *ab initio* parametrization of density functional dispersion correction (DFT-D) for the 94 elements H-Pu. The Journal of Chemical Physics 132(15), 154104 (2010). https://doi.org/10.1063/1.3382344

19. Hariharan, P.C., Pople, J.A.: The influence of polarization functions on molecular orbital hydrogenation energies. Theoretica Chimica Acta 28(3), 213–222 (1973). https://doi.org/10.1007/BF00533485

20. Hecker, S.J., Reddy, K.R., Lomovskaya, O., *et al.*: Discovery of Cyclic Boronic Acid QPX7728, an Ultrabroad-Spectrum Inhibitor of Serine and Metallo-β-lactamases. Journal of Medicinal Chemistry 63(14), 7491–7507 (2020). https://doi.org/10.1021/acs.jmedchem.9b01976

21. Hehre, W.J., Ditchfield, R., Pople, J.A.: Self-Consistent Molecular Orbital Methods. XII. Further Extensions of Gaussian-Type Basis Sets for Use in Molecular Orbital Studies of Organic Molecules. The Journal of Chemical Physics 56(5), 2257–2261 (1972). https://doi.org/10.1063/1.1677527

22. Hirshfeld, F.: Bonded-atom fragments for describing molecular charge densities. The Journal of Physical Chemistry A 44(2), 129–138 (1977). https://doi.org/10.1007/BF00549096

23. Huang, J., Rauscher, S., Nawrocki, G., *et al.*: CHARMM36m: an improved force field for folded and intrinsically disordered proteins. Nature Methods 14(1), 71–73 (2017). https://doi.org/10.1038/nmeth.4067

24. Humphrey, W., Dalke, A., Schulten, K.: VMD: Visual molecular dynamics. Journal of Molecular Graphics 14(1), 33–38 (1996). https://doi.org/10.1016/0263-7855(96)00018-5

25. Jorgensen, W.L., Chandrasekhar, J., Madura, J.D., *et al.*: Comparison of simple potential functions for simulating liquid water. The Journal of Chemical Physics 79(2), 926–935 (1983). https://doi.org/10.1063/1.445869

26. Krajnc, A., Brem, J., Hinchliffe, P., *et al.*: Bicyclic boronate VNRX-5133 inhibits metallo- and serine-β-lactamases. Journal of Medicinal Chemistry 62(18), 8544–8556 (2019). `https://doi.org/10.1021/acs.jmedchem.9b00911`

27. Krivitskaya, A.V., Khrenova, M.G.: Boronic Acids as Prospective Inhibitors of Metallo-β-Lactamases: Efficient Chemical Reaction in the Enzymatic Active Site Revealed by Molecular Modeling. Molecules 26(7), 2026 (2021). `https://doi.org/10.3390/molecules26072026`

28. Lence, E., González-Bello, C.: Bicyclic Boronate β-Lactamase Inhibitors: The Present Hope against Deadly Bacterial Pathogens. Advanced Therapeutics 4(5), 2000246 (2021). `https://doi.org/10.1002/adtp.202000246`

29. Lomovskaya, O., Tsivkovski, R., Nelson, K., *et al.*: Spectrum of beta-lactamase inhibition by the cyclic boronate QPX7728, an ultrabroad-spectrum beta-lactamase inhibitor of serine and metallo-beta-lactamases: enhancement of activity of multiple antibiotics against isogenic strains expressing single beta-lactamases. Antimicrobial Agents and Chemotherapy 64(6), e00212–20 (2020). `https://doi.org/10.1128/AAC.00212-20`

30. Lu, T., Chen, F.: Multiwfn: A multifunctional wavefunction analyzer. Journal of Computational Chemistry 33(5), 580–592 (2012). `https://doi.org/10.1002/jcc.22885`

31. MacKerell, A.D., Bashford, D., Bellott, M., *et al.*: All-Atom Empirical Potential for Molecular Modeling and Dynamics Studies of Proteins. The Journal of Physical Chemistry B 102(18), 3586–3616 (1998). `https://doi.org/10.1021/jp973084f`

32. MacKerell, A.D., Feig, M., Brooks, C.L.: Improved Treatment of the Protein Backbone in Empirical Force Fields. Journal of the American Chemical Society 126(3), 698–699 (2004). `https://doi.org/10.1021/ja036959e`

33. Mata, I., Alkorta, I., Espinosa, E., Molins, E.: Relationships between interaction energy, intermolecular distance and electron density properties in hydrogen bonded complexes under external electric fields. Chemical Physics Letters 507(1-3), 185–189 (2011). `https://doi.org/10.1016/j.cplett.2011.03.055`

34. Melo, M.C.R., Bernardi, R.C., Rudack, T., *et al.*: NAMD goes quantum: an integrative suite for hybrid simulations. Nature Methods 15(5), 351–354 (2018). `https://doi.org/10.1038/nmeth.4638`

35. Michaud-Agrawal, N., Denning, E.J., Woolf, T.B., Beckstein, O.: MDAnalysis: A toolkit for the analysis of molecular dynamics simulations. Journal of Computational Chemistry 32(10), 2319–2327 (2011). `https://doi.org/10.1002/jcc.21787`

36. Mojica, M.F., Rossi, M.A., Vila, A.J., Bonomo, R.A.: The urgent need for metallo-β-lactamase inhibitors: an unattended global threat. The Lancet Infectious Diseases 22(1), e28–e34 (2022). `https://doi.org/10.1016/S1473-3099(20)30868-9`

37. Novais, A., Ferraz, R.V., Viana, M., *et al.*: NDM-1 Introduction in Portugal through a ST11 KL105 *Klebsiella pneumoniae* Widespread in Europe. Antibiotics 11(1), 92 (2022). `https://doi.org/10.3390/antibiotics11010092`

38. Oláh, J., Van Alsenoy, C., Sannigrahi, A.B.: Condensed Fukui Functions Derived from Stockholder Charges: Assessment of Their Performance as Local Reactivity Descriptors. The Journal of Physical Chemistry A 106(15), 3885–3890 (2002). `https://doi.org/10.1021/jp014039h`

39. Osei Sekyere, J.: Current State of Resistance to Antibiotics of Last-Resort in South Africa: A Review from a Public Health Perspective. Frontiers in Public Health 4, 209 (2016). `https://doi.org/10.3389/fpubh.2016.00209`

40. Palacios, A.R., Rossi, M.A., Mahler, G.S., Vila, A.J.: Metallo-β-lactamase inhibitors inspired on snapshots from the catalytic mechanism. Biomolecules 10(6), a025239 (2020). `https://doi.org/10.3390/biom10060854`

41. Parkova, A., Lucic, A., Krajnc, A., *et al.*: Broad spectrum β-lactamase inhibition by a thioether substituted bicyclic boronate. ACS Infectious Diseases 6(6), 1398–1404 (2019). `https://doi.org/10.1021/acsinfecdis.9b00330`

42. Parkova, A., Lucic, A., Krajnc, A., *et al.*: A 2018-2019 patent review of metallo beta-lactamase inhibitors. ACS Infectious Diseases 30(7), 541–555 (2020). `https://doi.org/10.1080/13543776.2020.1767070`

43. Phillips, J.C., Hardy, D.J., Maia, J.D.C., *et al.*: Scalable molecular dynamics on CPU and GPU architectures with NAMD. The Journal of Chemical Physics 153(4), 044130 (2020). `https://doi.org/10.1063/5.0014475`

44. Phillips, L.C., Braun, R., Wang, W., *et al.*: Scalable molecular dynamics with NAMD. Journal of Computational Chemistry 26(16), 1781–1802 (2005). `https://doi.org/10.1002/jcc.20289`

45. Sabet, M., Tarazi, Z., Griffith, D.C.: *In vivo* activity of QPX7728, an ultrabroad-spectrum beta-lactamase inhibitor, in combination with beta-lactams against carbapenem-resistant Klebsiella pneumoniae. Antimicrobial Agents and Chemotherapy 64(11), e01267–20 (2020). `https://doi.org/10.1128/AAC.01267-20`

46. Santucci, M., Spyrakis, F., Cross, S., *et al.*: Computational and biological profile of boronic acids for the detection of bacterial serine- and metallo-β-lactamases. Scientific reports 7(17716), 1–15 (2017). `https://doi.org/10.1038/s41598-017-17399-7`

47. Seritan, S., Bannwarth, C., Fales, B.S., *et al.*: TeraChem: A graphical processing unitaccelerated electronic structure package for largescale ab initio molecular dynamics. Wiley Interdisciplinary Reviews: Computational Molecular Science 11(2), e1494 (2021). `https://doi.org/10.1002/wcms.1494`

48. Shahi, A., Arunan, E.: Hydrogen bonding, halogen bonding and lithium bonding: an atoms in molecules and natural bond orbital perspective towards conservation of total bond order, inter- and intra-molecular bonding. Physical Chemistry Chemical Physics 16(4), 22935–22952 (2014). `https://doi.org/10.1039/C4CP02585G`

49. Shi, C., Chen, J., Kang, X., *et al.*: Approaches for the discovery of metallo-β-lactamase inhibitors: A review. Chemical Biology & Drug Design 94(2), 1427–1440 (2019). `https://doi.org/10.1111/cbdd.13526`

50. Tehrani, K.H., Martin, N.I.: β-lactam/β-lactamase inhibitor combinations: an update. MedChemComm 9(9), 1439–1456 (2018). `https://doi.org/10.1039/c8md00342d`

51. Thapa, S., Adhikari, N., Shah, A.K., *et al.*: Detection of NDM-1 and VIM genes in carbapenem-resistant *Klebsiella pneumoniae* isolates from a tertiary health-care center in Kathmandu, Nepal. Chemotherapy 66(5-6), 199–209 (2021). `https://doi.org/10.1159/000518256`

52. Tooke, C.L., Hinchliffe, P., Bragginton, E.C., *et al.*: Lactamases and β-Lactamase Inhibitors in the 21st Century. Journal of Molecular Biology 431(18), 3472–3500 (2019). `https://doi.org/10.1016/j.jmb.2019.04.002`

53. Tsivkovski, R., Totrov, M., Lomovskaya, O.: Biochemical characterization of QPX7728, a new ultrabroad-spectrum beta-lactamase inhibitor of serine and metallo-beta-lactamases. Antimicrobial Agents and Chemotherapy 64(6), e00130–20 (2020). `https://doi.org/10.1128/AAC.00130-20`

54. Valiev, M., Bylaska, J., Govind, N., *et al.*: NWChem: A comprehensive and scalable open-source solution for large scale molecular simulations. Computer Physics Communications 181(9), 1477–1489 (2010). `https://doi.org/10.1016/j.cpc.2010.04.018`

55. Vanommeslaeghe, K., Hatcher, E., Acharya, C., *et al.*: CHARMM general force field: A force field for drug-like molecules compatible with the CHARMM all-atom additive biological force fields. Journal of Computational Chemistry 31(4), 671–690 (2009). `https://doi.org/10.1002/jcc.21367`

56. Vanquelef, E., Simon, S., Marquant, G., *et al.*: R.E.D. Server: a web service for deriving RESP and ESP charges and building force field libraries for new molecules and molecular fragments. Nucleic Acids Research 39, W511–W517 (2011). `https://doi.org/10.1093/nar/gkr288`

57. Vázquez-Ucha, J.C., Rodríguez, D., Lasarte-Monterrubio, C., *et al.*: 6-Halopyridylmethylidene Penicillin-Based Sulfones Efficiently Inactivate the Natural Resistance of *Pseudomonas aeruginosa* to β-Lactam Antibiotics. Journal of Medicinal Chemistry 64(9), 6310–6328 (2021). `https://doi.org/10.1021/acs.jmedchem.1c00369`

58. Venkata, K.C.N., Ellebrecht, M., Tripathi, S.K.: Efforts towards the inhibitor design for New Delhi metallo-beta-lactamase (NDM-1). European Journal of Medicinal Chemistry 225(5), 113747 (2021). `https://doi.org/10.1016/j.ejmech.2021.113747`

59. Voevodin, V.V., Antonov, A.S., Nikitenko, D.A., *et al.*: Supercomputer Lomonosov-2: Large Scale, Deep Monitoring and Fine Analytics for the User Community. Supercomputing Frontiers and Innovations 6(2), 4–11 (2019). `https://doi.org/10.14529/jsfi190201`

60. Yu, W., He, X., Vanommeslaeghe, K., MacKerell, A.D.: Extension of the CHARMM general force field to sulfonyl-containing compounds and its utility in biomolecular simulations. Journal of Computational Chemistry 33(31), 2451–2468 (2012). `https://doi.org/10.1002/jcc.23067`